

Parallel Converter-based Hybrid HVDC System for Integration and Delivery of Large-scale Renewable Energy

Hanlin Guo, Zheren Zhang, *Member, IEEE*, and Zheng Xu, *Fellow, IEEE*

Abstract—In this study, a novel parallel converter-based hybrid high-voltage direct current (HVDC) system is proposed for the integration and delivery of large-scale renewable energy. The rectifier uses the line commutated converter (LCC) and low-capacity modular multilevel converter (MMC) in parallel, while the inverter uses MMC. This configuration combines the economic advantages of LCC with the flexibility of MMC. Firstly, the steady-state control strategies are elaborated. The low-capacity MMC operates in the grid-forming mode to offer AC voltage support. It also provides active filtering for the LCC and maintains the reactive power balance of the sending-end system. The LCC efficiently transmits all active power at the rectifier side, fully exploiting its bulk-power transmission capability. Secondly, the fault ride-through strategies of both the AC faults at two terminals and the DC fault are proposed, in which the MMCs at both terminals can remain unblocked under various faults. Thus, the proposed system can mitigate the impact of the faults and ensure continuous voltage support for the sending-end system. Finally, simulations in PSCAD/EMTDC verify the effectiveness and performance of the proposed system.

Index Terms—Line commutated converter (LCC), modular multilevel converter (MMC), grid-forming, parallel converter, high-voltage direct current (HVDC), renewable energy.

I. INTRODUCTION

IN response to the challenges of climate change and ever-increasing energy demand, China has strategically planned several large-scale renewable energy bases (REBs) in its western regions. Given that load centers in China are predominantly situated in the eastern regions, the high-voltage direct current (HVDC) technology is envisioned to play a pivotal role in the long-distance and bulk-capacity transmission for these REBs [1], [2].

Presently, two collection schemes are available for REBs: AC collection [3] and DC collection [4]. The AC collection scheme uses the grid-connected inverter as the interface for

the generation unit, which can then be connected to the rectifier station of the HVDC system via AC lines. In the DC collection scheme, pure DC configurations are adopted for the REB. Under current technical conditions, the AC collection scheme is a more mature option and is thus studied in this paper. As for the HVDC systems, the line commutated converter (LCC) and modular multilevel converter (MMC) are two mainstream types of converters implemented in practical projects. The LCC features technological maturity, cost-effective investments, and low energy losses. However, it relies on the external AC voltage source to provide its commutation voltage and is not capable of offering voltage support for REBs [5], [6]. Although REBs can theoretically operate in the grid-forming mode [7], there are few such installations worldwide and the associated operational experience remains relatively limited. Grid-following converters are likely to remain the primary choice for renewable energy generations in short-term future projects [8], [9]. Additionally, the LCC has issues of excessive reactive power consumption, poor power quality, and potential commutation failures. In contrast, the MMC has independent grid-forming capability and does not suffer from commutation failures [10]. This technology also eliminates the massive harmonic filters and reactive power compensation devices. However, it does come with higher power losses and investment costs, making it less economically viable for GW-level power transmission [11]. Therefore, the pure LCC- or MMC-HVDC system is not the best choice for the integration and delivery of large-scale renewable energy. To fully utilize the advantages of both converters, various hybrid HVDC systems have been proposed, categorized as the terminal-based hybrid, the pole-based hybrid, and the converter-based hybrid schemes [12]–[14].

In terminal-based hybrid schemes, LCC and MMC are used at different terminals [15]. It has been applied in the Wudongde project in China, where an LCC terminal operates as the rectifier and two MMC terminals operate as the inverters [16]. In this project, the hybrid-submodule MMC that combines full-bridge submodules and half-bridge submodules is adopted. It can deal with DC faults compared to the half-bridge submodule MMC, while its manufacturing cost and operation loss are lower than those of the full-bridge submodule MMC. This configuration (LCC used as the rectifier) does not suffer from commutation failures. Nev-

Manuscript received: December 29, 2023; revised: March 11, 2024; accepted: April 29, 2024. Date of CrossCheck: April 29, 2024. Date of online publication: May 31, 2024.

This work was supported by the Science and Technology Projects of State Grid Corporation of China (No. 5200-202356402A-2-4-KJ).

This article is distributed under the terms of the Creative Commons Attribution 4.0 International License (<http://creativecommons.org/licenses/by/4.0/>).

H. Guo, Z. Zhang (corresponding author), and Z. Xu are with the Department of Electrical Engineering, Zhejiang University, Hangzhou, China (e-mail: guo-hanlin@zju.edu.cn; 3071001296zhang@zju.edu.cn; xuzheng007@zju.edu.cn).

DOI: 10.35833/MPCE.2023.001033



ertheless, if it is applied to transmitting large-scale renewable energy, the absence of voltage support for REBs will cause operation issues.

The pole-based hybrid scheme uses LCC and MMC in different poles. A typical application is the Skagerrak HVDC project connecting the Norwegian grid and the Danish grid [17]. For this scheme, the risk of commutation failures still exists on the inverter side of the LCC link. This scheme can be used to upgrade the existing monopolar LCC-HVDC systems but is not particularly suitable for the power transmission of newly planned large-scale REBs.

In the converter-based hybrid scheme, LCC and MMC are combined in the same pole of the same converter station, which can be connected in series or in parallel. The series converter-based hybrid scheme has been studied widely [18]-[21] and applied in the Baihetan-Jiangsu project in China [22], [23]. For the transmission of large-scale renewable energy, [19] proposes the scheme of using series hybrid converter comprising LCC and MMC for both the rectifier and inverter. In this scheme, the DC fault ride-through can be realized with the LCC force retardation. However, the risk of commutation failures cannot be avoided completely. To address this problem, [20] proposes the scheme of using series hybrid converter comprising LCC and MMC only in the rectifier, while using MMC in the inverter. It installs diodes on the overhead lines to cut off DC fault currents from the inverter, but this causes additional power losses. In [21], diodes on the overhead lines are eliminated and hybrid-submodule MMCs are used in the inverter to deal with the DC fault. Overall, the above series schemes ensure the AC voltage support for the sending-end grid and improve the performance of the HVDC system. However, the power reversal for these systems is inconvenient since the current direction of the LCC cannot be changed, and the black start of the sending-end system that consists of pure REBs is difficult.

The static synchronous compensator (STATCOM) may also be used in cooperation with the LCC for the integration of REBs. But it also has difficulties in the black start. Besides, the STATCOM needs to adopt the grid-forming control mode on the AC side and the DC voltage (submodule capacitor voltage) control mode on the DC side, which is more complex, and the performance under large disturbances has yet to be evaluated. By contrast, the parallel converter-based hybrid system allows LCC and MMC to flow different DC currents. Therefore, the black start can easily be realized by making the MMC at the sending-end operate in the inverter mode. It can enhance the flexibility of the HVDC system while fully utilizing the transmission capability of the LCC [12]. Unfortunately, little research has focused on the parallel scheme, and several challenges remain in connecting different types of converters to the single bus. On the one hand, the parallel MMC should be reliable enough, to continuously provide commutation voltage for the LCC on the same bus and the voltage reference for the grid-connected inverter in the REB. It should remain unblocked as much as possible under different operating conditions. On the other hand, the classical control strategies for each converter have different mechanisms and effects. Thus, the control strategies

must be redesigned to ensure the coordinated operation, including the desired steady-state power distribution between different converters and fault ride-through. Therefore, this paper aims at the parallel converter-based hybrid HVDC system suitable for the integration and delivery of large-scale renewable energy. The main contributions are summarized as follows.

1) For the scenario where the sending-end system is pure REB, a parallel converter-based hybrid HVDC system is proposed. Its rectifier uses LCC and low-capacity MMC in parallel, while its inverter uses MMC. Fixed capacitors are also equipped on the AC side of the rectifier to provide partial reactive power compensation for the LCC. This configuration combines the technical and economic advantages of LCC and MMC, demonstrating potential feasibility for engineering implementation under current technological conditions. Besides, the selection method of the rated capacity of the converter is elaborated.

2) The steady-state and fault ride-through control strategies are designed for this system. In the steady state, the LCC efficiently transmits all active power on the rectifier side, since its manufacturing cost and power losses are lower than the MMC; the MMC in the rectifier station offers AC voltage support for the sending-end system. Under AC or DC temporary faults, the MMCs at both terminals can remain unblocked, which reduces the impacts of faults and ensures continuous voltage support.

The rest of this paper is structured as follows. Section II introduces the basics of the proposed system, including the system topology and the rated capacity selection of converters. Section III proposes the control strategies of the proposed system. In Section IV, case studies are conducted based on PSCAD/EMTDC. Section V draws the conclusions.

II. BASICS OF PROPOSED SYSTEM

A. System Topology

Figure 1 illustrates the topology of the proposed system. For simplicity, only the positive pole is presented.

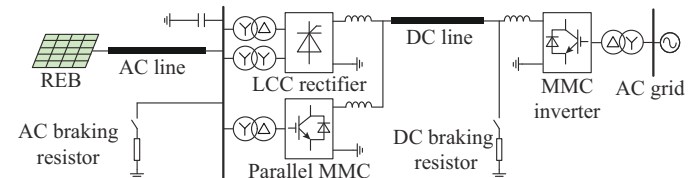


Fig. 1. Topology of proposed system.

Also, because of the requirements for bulk capacity and high-voltage level, each converter in Fig. 1 may actually consist of multiple basic units in cascade. The REB is represented by the AC collection photovoltaic (PV) systems in this paper. It uses the single-stage inverter [24] and is connected to the rectifier station through AC lines. Then, the active power is transmitted to the receiving-end AC grid by the LCC rectifier, the DC lines, and the MMC inverter. Another MMC is connected in parallel with the LCC at the rectifier side. To reduce the cost while retaining the technical

advantages of full-bridge submodules, both MMCs in the rectifier and the inverter adopt the hybrid-submodule MMC. Under the control of LCC, no active power from the REB needs to be transmitted through the parallel MMC on the rectifier side, reducing its rated capacity and minimizing converter power losses. The functions of the parallel MMC are as follows:

1) The AC voltage of the sending-end AC grid is controlled by the parallel MMC. Therefore, the commutation voltage for the LCC is available, and the grid-following converters with high technological maturity can be applied in the REB.

2) The reactive power balance of the sending-end AC grid is maintained by the parallel MMC. Specific capacity selection methods are described in the next subsection.

3) The parallel MMC also behaves as an active power filter on the AC side, and the AC harmonic currents generated by the LCC are filtered by it. As a result, the bulky AC filter banks can be eliminated.

Additionally, for fault ride-through purposes, DC braking resistors and AC braking resistors are installed at the DC side of the inverter and the AC side of the rectifier, respectively. Specific configuration principles and control strategies for these braking resistors are introduced in Section III-C and Section III-D.

B. Rated Capacity Selection of Converters

1) LCC Rectifier and MMC Inverter

The LCC rectifier and MMC inverter are required to transmit the full active power, and their rated capacities are selected as the rated capacity of the REB.

2) Parallel MMC

The rated capacity of the parallel MMC can be expressed as:

$$S_{\text{MMC}} = S_Q + S_h + kS_{\text{LCC}} \quad (1)$$

where S_Q and S_h are the capacities for reactive power balance and harmonic suppression, respectively; and kS_{LCC} denotes the capacity margin using the capacity of the LCC S_{LCC} as the reference, and the margin coefficient k can be taken as 0.1.

In the sending-end system, the reactive power is mainly consumed by the LCC. As a compromise, and considering that the MMC can both supply or consume the reactive power, S_Q is designed based on the principle that the maximum reactive power consumption of the LCC is supplied by half of the parallel MMC and half of the fixed capacitors. In this way, the capacity of the parallel MMC can be reduced and the reactive power balance of the system can be achieved flexibly at different power levels. For example, when the reactive power consumption is low, the parallel MMC can also absorb reactive power to achieve balance. Note that although the AC lines may also consume or generate reactive power, it is not very high and there is sufficient capacity margin left for the parallel MMC. Therefore, the reactive power balance can still be achieved.

The reactive power consumption of the LCC rectifier Q_{LCC} is:

$$Q_{\text{LCC}} = \frac{3U_r^2}{4\pi X_T T^2} (2\mu + \sin(2\alpha) - \sin(2\alpha + 2\mu)) \quad (2)$$

where U_r is the root mean square value of the sending-end AC voltage; X_T and T are the leakage reactance and the transformer ratio of the LCC converter transformer, respectively; and α and μ are the firing angle and overlap angle of the LCC, respectively, and μ can be calculated by:

$$\mu = \pi - \alpha - \arccos\left(\frac{\sqrt{2} I_d X_T T}{E} + \pi - \alpha\right) \quad (3)$$

where I_d is the DC current flowing through the LCC; and E is the line-to-line voltage of the sending-end AC bus.

The analysis results in [25] show that 5% of the capacity of the LCC is sufficient for harmonic suppression. It should be noted that the AC filter banks are much cheaper than the MMC, but they have a larger footprint. For some REBs such as the PV bases in the desert of western China, the area suitable for the construction of the rectifier station may be severely constrained by the challenging terrain. Therefore, eliminating the AC filter banks in such scenarios can save the investment cost of the whole station.

Take a bipolar HVDC system with the rated capacity of 10000 MW as an example. Its basic parameters are listed in Table I, and both the positive pole and negative pole consist of two series 12-pulse LCCs.

TABLE I
BASIC PARAMETERS OF A BIPOLAR HVDC SYSTEM

Parameter	Value
DC voltage	±800 kV
AC voltage	500 kV
Capacity of transformer	1500 MW (for each 6-pulse LCC)
Transformer ratio	500 kV/165 kV
Transformer leakage reactance	0.15 p.u.

Assume that α is set to be 15° . In this case, the active power transmitted is approximated to be 10000 MW. According to (2) and (3), the total reactive power consumed by LCCs in the positive and negative poles is 4895 Mvar, which is about 50% of the system capacity. Therefore, S_Q is about $0.25S_{\text{LCC}}$ and S_{MMC} can be selected as $0.4S_{\text{LCC}}$ in this example.

III. CONTROL STRATEGIES OF PROPOSED SYSTEM

A. Steady-state Control

1) LCC Rectifier

The control block diagram of the LCC rectifier is shown in Fig. 2, where P_{MMC} is the active power flowing from the AC side into the parallel MMC; and i_{LCCref} and i_{LCC} are the reference and measured values of the DC current of the LCC, respectively. Firstly, the classical DC current control and the minimum firing angle (5°) control for the LCC rectifier are adopted. Then, the active power control is used to keep the active power of the parallel MMC at zero, which means that all active power on the rectifier side can be trans-

mitted through the LCC. Additionally, for the bipolar HVDC system, since each LCC only aims at controlling the active power of the parallel MMC in its respective pole to zero, the power balance between the positive and negative poles cannot be ensured. To deal with this problem, the power balance control depicted in Fig. 3 is applied in the steady state, where P_{LCCpos} and P_{LCCneg} are the active power of the positive and negative LCCs, respectively. The power difference is passed through a proportional-integral (PI) controller to generate a modified value of the DC current reference, i. e., Δi_{LCCref} . The inputs of the positive and negative DC current controllers of the LCC are subtracted or added to Δi_{LCCref} respectively.

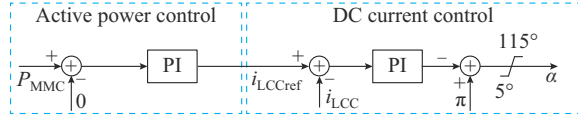


Fig. 2. Control block diagram of LCC rectifier.

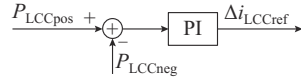


Fig. 3. Control block diagram of power balance control.

2) Parallel MMC

Figure 4 presents the control block diagram of the parallel MMC. u_{aref} and i_{ref} are the references for the AC voltage of the rectifier station and the AC output current of the parallel MMC, respectively. Their corresponding measured values are u_{ac} and i_{MMC} , respectively. i_{rec} is the measured value of AC current flowing out from the rectifier station, including the LCC and the parallel MMC. The subscripts d and q denote the d -axis and q -axis components of corresponding variables, respectively. The fundamental phase θ_0 is the integral of the fundamental angular frequency ω_0 . h is the order of the harmonic. m_{dm} is the differential mode modulation signal of the MMC.

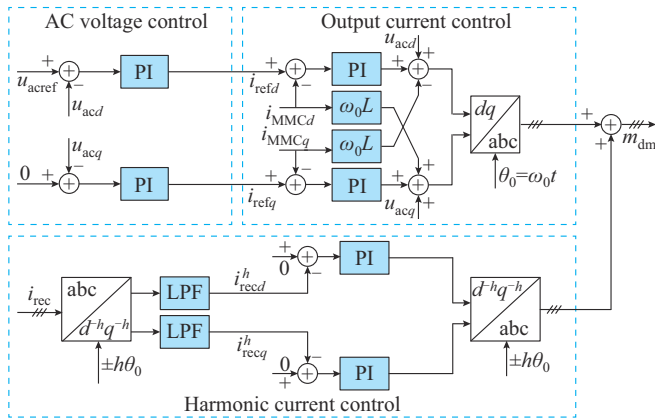
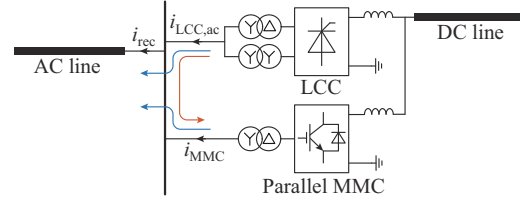


Fig. 4. Control block diagram of parallel MMC.

On the one hand, the AC voltage control and the output current control compose the dual closed-loop control to establish the voltage amplitude and frequency of the sending-end AC grid.

On the other hand, the harmonic current control is de-

signed to make the total output current of the rectifier station i_{rec} free of harmonics. Figure 5 presents the mechanism of harmonic current control. $i_{LCC,ac}$ is the AC current of the LCC. For the 12-pulse LCC, its main harmonic currents on the AC side are of the $(12k \pm 1)^{th}$ order ($k=1,2,\dots$). Therefore, the parallel MMC will actually generate harmonic currents of the $(12k \pm 1)^{th}$ order, whose phases are opposite to those in $i_{LCC,ac}$. That is, the filtering of the total output current of the rectifier station is achieved by compensating for the harmonic currents of the LCC.



← Total current; ← Fundamental current; ← Harmonic current

Fig. 5. Mechanism of harmonic current control.

Besides, sequences of the $(3k-2)^{th}$, $(3k-1)^{th}$, and $(3k)^{th}$ harmonics are positive, negative, and zero, respectively. Therefore, the transformation matrix expressed as (4) is adopted to extract the h^{th} harmonic current. It can transform variables in the three-phase static frame to the $d^h q^h$ rotating frame, where the rotating direction depends on the sequence of the h^{th} harmonic.

$$T_{abc-dq}(\pm h\theta_0) = \frac{2}{3} \begin{bmatrix} \cos(\pm h\theta_0) & \cos(\pm h\theta_0 - \frac{2}{3}\pi) & \cos(\pm h\theta_0 + \frac{2}{3}\pi) \\ -\sin(\pm h\theta_0) & -\sin(\pm h\theta_0 - \frac{2}{3}\pi) & -\sin(\pm h\theta_0 + \frac{2}{3}\pi) \end{bmatrix} \quad (4)$$

After the transformation in (4), the h^{th} harmonic current becomes a DC component in the $d^h q^h$ rotating frame, while other currents become AC components and can be filtered by the low-pass filters (LPFs). PI controllers are then used to generate the corresponding modulation signals to realize the current compensation.

Other basic controllers for MMC, such as the circulating current control, are omitted in Fig. 4.

3) MMC Inverter

The MMC inverter adopts the regular dual closed-loop constant DC voltage control. Its control block diagram can be found in [18] and will not be repeated in this paper.

B. AC Fault Control at Sending End

When a short-circuit fault occurs at the sending-end AC grid, the AC voltage of the rectifier station drops rapidly. This leads to a drop in the DC voltage of the LCC, as well as a reduction in its power transmission capability.

On the one hand, the drop in the DC voltage of the LCC may cause a drop in the DC current or even a reversal of its direction. The power transmitted from the sending-end to the receiving end can thus be reduced or even reversed. To avoid reverse power transmission as much as possible and

mitigate the impact on the receiving end, the backup DC current control shown in Fig. 6 is adopted in the MMC inverter. It uses i_{LCCref} minus a margin as its reference and generates the DC voltage reference u_{dcref2} based on the deviation of the DC current. By reference to the backup DC current control of the inverter in the classical LCC-HVDC system, this margin is taken to be 0.1 p.u. [18], [26]. The smaller value between u_{dcref2} and u_{dcref1} (provided by the upper-level controller) is selected for the following DC voltage control. In the steady state, the measured value of DC current (injected into the inverter) i_{dc} is greater than $i_{LCCref}-0.1$, so u_{dcref2} is its upper limit value and will not be selected. The backup DC current control is not effective at this time. When i_{dc} decreases due to the sending-end AC fault, u_{dcref2} also decreases and is selected. Consequently, the inverter is able to reduce the DC voltage to maintain the DC current.

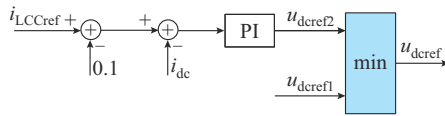


Fig. 6. Backup DC current control of MMC inverter.

On the other hand, the surplus power will cause the DC voltage of the grid-connected inverters in the REB to increase. However, the PV units can reduce their output power quickly in response to changes of the DC voltage, so that severe overvoltage will not occur. In view of this, no additional power dissipation measures are needed.

C. AC Fault Control at Receiving End

When a short-circuit fault occurs at the receiving-end AC grid, the AC voltage of the MMC inverter drops rapidly which impedes its power output to the AC side. The surplus power results in the increase of the DC voltage. Given the inevitable long delay in the long-distance transmission of the fault detection signal, it is challenging to coordinate the sending-end system to reduce the power, resulting in a constrained performance. Therefore, the chopper-controlled braking resistor, with a total capacity equal to the rated DC power of the system, is installed at the DC side of the MMC inverter. It is inserted to dissipate the surplus power when the DC voltage exceeds the preset upper threshold, and is blocked when the DC voltage drops below the preset lower threshold.

D. DC Fault Control

For the DC fault, two issues need to be addressed. On the one hand, the power delivery capability of the HVDC system is degraded and the surplus power of the sending-end AC grid needs to be dissipated. On the other hand, the control strategies of the converters need to be designed to achieve DC fault clearing and system recovery. For the first issue, braking resistors are installed at the AC side of the rectifier, which are set in groups with a total capacity equal to that of the REB. They are inserted and blocked according to the DC fault detection signal. For the second issue, the fault ride-through strategies are as follows.

1) Rectifier

Both the LCC and the parallel MMC that consists of hybrid-submodules can generate negative DC voltages to clear DC fault currents. However, due to their different control mechanisms and schemes, it is difficult to coordinate them to output the same DC voltage during the fault. In view of this, this paper adopts the strategy of blocking the LCC during the DC fault and clearing fault currents only with the parallel MMC.

For the LCC, it is immediately blocked when the DC fault is detected. After the fault has been cleared, it remains blocked for another 200 ms waiting for the deionization. Then, it is unlocked and the firing angle is controlled to decrease linearly from 45° to 15° within 200 ms. Finally, it is switched to the steady-state control strategy. The fault occurrence is judged by detecting the DC current exceeding 1.5 p.u..

As for the parallel MMC, its fault ride-through strategy under DC fault is shown in Fig. 7. When the DC fault is detected, the DC current control is enabled. It generates the DC voltage reference u_{dcref} for modulation based on the DC current reference (set to be zero) and its measured value i_{dc} . m_{cm} is the common mode modulation signal. m_u and m_l are the modulation signals for the upper arm and lower arm, respectively. The subscript j ($j=a, b, c$) indicates the corresponding phase.

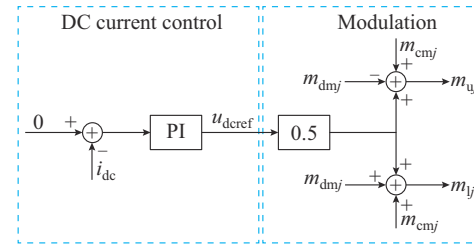


Fig. 7. Fault ride-through strategy of parallel MMC under DC fault.

In addition, to maintain the submodule capacitor voltage of the parallel MMC in the fault pole during the fault, one group of AC braking resistors is selected for control according to the average voltage of the submodule capacitors u_{cave} , which is calculated by:

$$u_{cave} = \frac{1}{6Nu_{cN}} \sum_{j=a,b,c} \sum_{k=u,l} \sum_{x=1}^N u_c(j,k,x) \quad (5)$$

where $u_c(j,k,x)$ is the voltage of the x^{th} submodule capacitor on arm k in phase j ; N is the number of submodules in one arm; and u_{cN} is the nominal voltage of the submodule capacitor. The selected group of AC braking resistors is inserted when u_{cave} exceeds the preset upper threshold, and is blocked when u_{cave} drops below the preset lower threshold. In this way, the parallel MMC can remain the grid-forming mode during the DC fault, thus mitigating the impact on the AC systems and offering continuous voltage support for the REB.

2) Inverter

The MMC inverter also adopts the DC current control shown in Fig. 7 to clear fault currents. Besides, since it operates in the grid-following control mode, its d -axis control can be switched to the capacitor voltage control without hav-

ing to utilize the braking resistor. The complete ride-through strategy of the MMC inverter under DC fault is illustrated in Fig. 8, where u_{cref} is the reference for the average voltage of the submodule capacitors; and Q_{ref} is the reference for the reactive power control. The capacitor voltage control employs the PI controller and generates the reference for the d -axis current based on the deviation of the average voltage of the submodule capacitors.

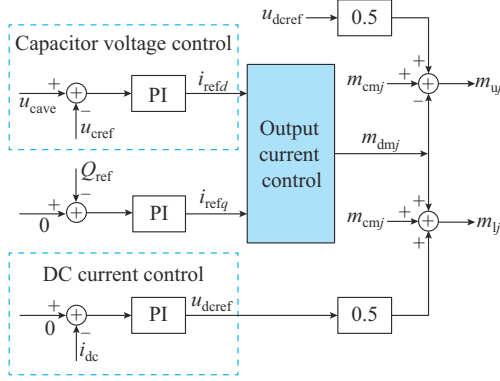


Fig. 8. Ride-through strategy of MMC inverter under DC fault.

IV. CASE STUDY

To verify the effectiveness and performance of the proposed system, a simulation case is established in PSCAD/EMTDC. In the case system, the PV-based REB is rated at 10000 MW and the HVDC system is a 10000 MW/ ± 800 kV symmetrical bipolar system. Each pole of the rectifier station consists of two series 12-pulse LCCs and two series hybrid-submodule MMCs, while each pole of the inverter station consists of two series hybrid-submodule MMCs. Note that with the maximum capability of insulated gate bipolar transistor (IGBT) in existing projects, each pole of the inverter station requires two series 1250 MW/400 kV MMCs (as a set) and then two sets in parallel. Since the MMCs at the receiving end are located in the same inverter station and share the same AC bus of the inverter station (joint station construction scheme), each pole is represented by two equivalent series 2500 MW/400 kV MMCs in the simulation to improve the simulation efficiency. The length of DC overhead lines is 2000 km and the frequency-dependent (phase) model is adopted in the simulation. Other main parameters of the simulation system are listed in Table II.

A. Power Fluctuation of Renewable Energy

Figure 9 presents the system response when the output power of the REB fluctuates, where an equivalent 1000 MW PV generation unit is tripped at $t = 2.0$ s.

According to Fig. 9, the LCC absorbs all the fluctuating active power and controls the active power injected into the parallel MMC to keep it at zero. The parallel MMC can provide the reactive power compensation for the LCC and keep the reactive power balance of the sending-end AC grid automatically. Overall, the system can smoothly transition to a new stable operating point when the active power generated by the PV system fluctuates, which verifies the effectiveness of the proposed steady-state control strategies.

TABLE II
MAIN PARAMETERS OF SIMULATION SYSTEM

Item	Parameter	Value
LCC rectifier (each 6-pulse LCC)	Rated capacity of transformer	1500 MVA
	Transformer ratio	500 kV/165 kV
	Transformer leakage inductance	0.15 p.u.
Parallel MMC (one of the series MMCs)	Rated capacity of converter	1000 MVA
	Rated capacity of transformer	1200 MVA
	Rated DC voltage	400 kV
Parallel MMC (one of the series MMCs)	Transformer ratio	500 kV/210 kV
	Transformer leakage inductance	0.15 p.u.
	Number of full-bridge submodules per arm	140
	Number of half-bridge submodules per arm	60
	Submodule capacitor	16.7 mF
	Arm inductance	30.4 mH
MMC inverter one of the series MMCs)	DC inductor	0.3 H
	Rated capacity of converter	2500 MVA
	Rated capacity of transformer	3000 MVA
MMC inverter one of the series MMCs)	Rated DC voltage	400 kV
	Transformer ratio	500 kV/210 kV
	Transformer leakage inductance	0.15 p.u.
	Number of full-bridge submodules per arm	140
	Number of half-bridge submodules per arm	60
	Submodule capacitor	41.7 mF
Sending-end AC grid	Arm inductance	12.2 mH
	Rated AC voltage	500 kV
	Capacity of compensation capacitor banks	2500 Mvar
Receiving-end AC grid	Length of AC lines	50 km
	Rated AC voltage	500 kV
	Short-circuit ratio	5
	Impedance angle	80°

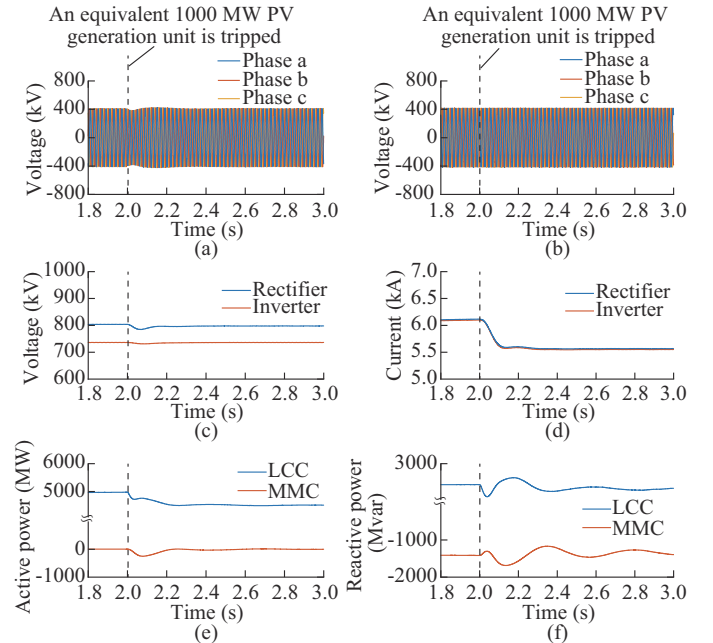


Fig. 9. System response to output power fluctuation of REB. (a) Sending-end AC voltage. (b) Receiving-end AC voltage. (c) DC voltage. (d) DC current. (e) Active power of positive-pole rectifier. (f) Reactive power of positive-pole rectifier.

B. AC Harmonic Filtering at Sending End

The AC harmonic currents generated by the 12-pulse LCC are mainly of the 11th, 13th, 23rd, and 25th orders. Therefore, the harmonic current control in the parallel MMC is designed for these four orders of harmonics. Figure 10 presents the harmonic characteristics of the positive-pole rectifier without and with the application of the harmonic current control.

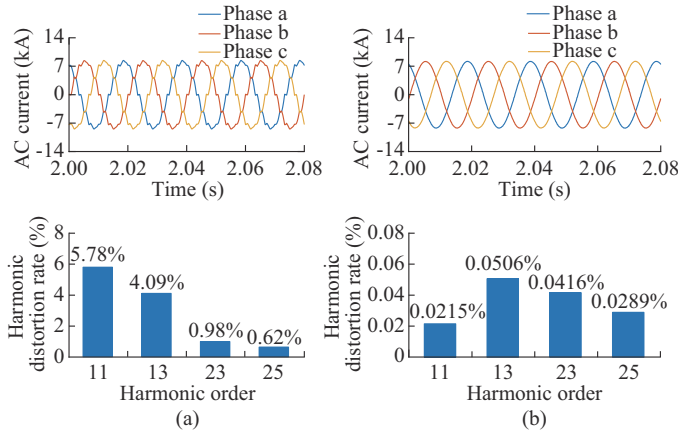


Fig. 10. Harmonic characteristics of positive-pole rectifier without and with application of harmonic current control. (a) Without application of harmonic current control. (b) With application of harmonic current control.

Without the application of the harmonic current control, the AC current of the rectifier station is severely distorted. In the IEEE Std 519, the maximum distortion limit is ranged from 0.5% to 1.5% for the 11th and 13th harmonic currents, and from 0.15% to 0.45% for the 23rd and 25th harmonic currents, depending on the operating conditions [27]. Therefore, the harmonic currents generated by the rectifier seriously exceed the limits, which is detrimental to the operation of the REB. In contrast, the waveform quality is greatly improved with the application of the harmonic current control in the parallel MMC. The distortion rates of each harmonic current are limited to a satisfactory level. Figure 11 is the harmonic characteristics of the positive-pole parallel MMC with the application of the harmonic current control. It can be observed that the parallel MMC does effectively absorb the harmonic currents output from the LCC.

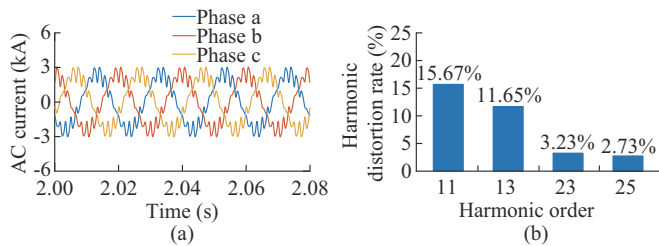


Fig. 11. Harmonic characteristic of positive-pole parallel MMC with application of harmonic current control. (a) AC current waveform of positive-pole parallel MMC. (b) Harmonic distortion rate.

In conclusion, the proposed harmonic current control for the parallel MMC is effective and can compensate for the harmonic currents output from the LCC well.

C. AC Fault at Sending End

The sending-end AC faults, including balanced and unbalanced faults, are assumed to occur on the AC side of the rectifier and the AC side of the PV inverter. The system responses are shown in Fig. 12 and Fig. 13. In both scenarios, the system operates stably before $t=2$ s. Then, the solid single-phase and three-phase faults occur at $t=2$ s. The fault durations are both 100 ms.

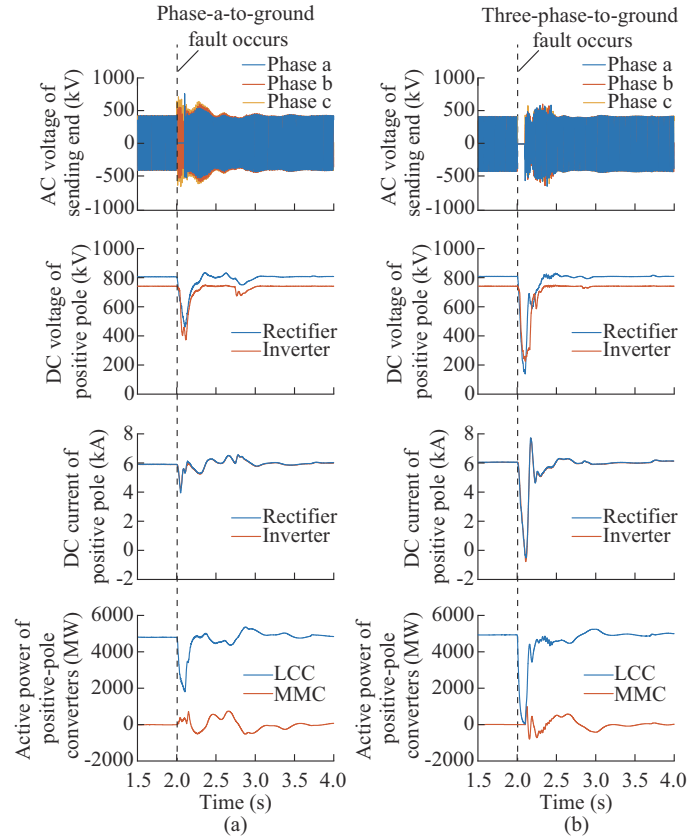


Fig. 12. System responses to AC faults at AC side of rectifier. (a) Scenario 1: phase-a-to-ground fault. (b) Scenario 2: three-phase-to-ground fault.

Based on Fig. 12 and Fig. 13, after the fault occurs, the voltage of the fault phase drops to zero. Due to the voltage relationship between the AC and DC sides of the LCC, the DC voltage of the rectifier station also drops and causes a drop in the DC current. However, the MMC inverter equipped with the backup DC current control is able to automatically reduce its DC voltage after the drop in DC current is detected. As a result, even in the case of a three-phase fault at the sending-end, there is no high reverse DC current, i.e., the HVDC system would not suffer from a large reverse power transmission. After the fault is cleared, the parallel MMC is able to reconstruct the voltage of the sending-end AC grid, and the system is able to return to steady-state operation quickly. Therefore, the proposed system can cope with various temporary faults of the sending-end AC grid.

D. AC Fault at Receiving End

The system responses to receiving-end AC faults, including balanced and unbalanced faults, are illustrated in Fig. 14. In both scenarios, the system operates stably before $t=2$ s.

Then, the solid single-phase and three-phase faults occur at $t=2$ s. The fault durations are both 100 ms. The upper and lower thresholds of the DC chopper in the simulations are set to be 800 kV and 736 kV, respectively.

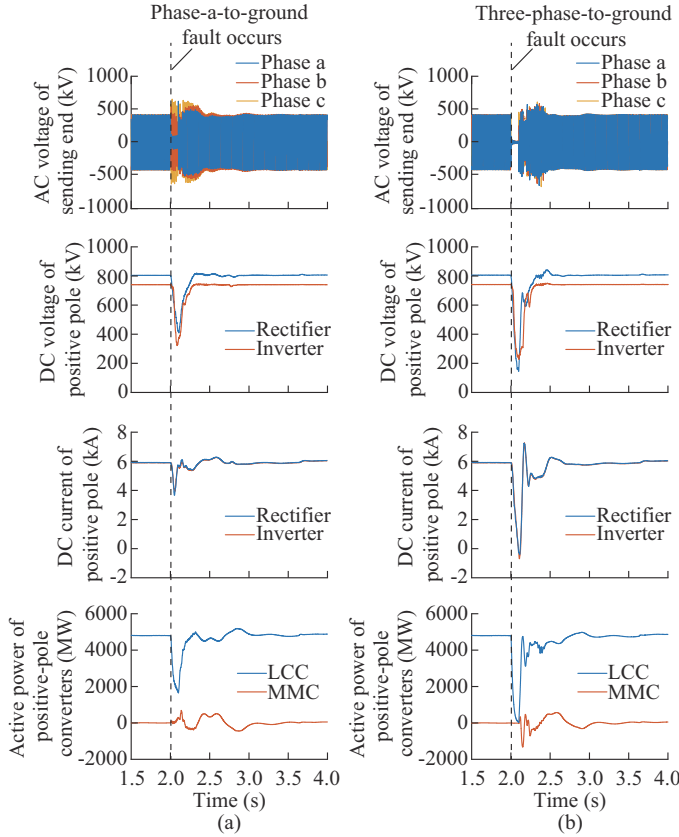


Fig. 13. System responses to AC faults on AC side of PV inverter. (a) Scenario 1: phase-a-to-ground fault. (b) Scenario 2: three-phase-to-ground fault.

According to Fig. 14, after the fault occurs, the AC voltage of the fault phase drops to zero, so the power output from the inverter to the receiving-end AC grid is impeded. Since the power of the REB is still continuously delivered to the HVDC system, the DC voltage rises and the DC dynamic braking resistors are put in. It can be observed that the braking resistors have frequent switching processes according to their current waveforms. The DC voltage also fluctuates due to the frequent switching processes of the braking resistors but is generally maintained within the appropriate range. In addition, the DC current flowing into the inverter drops significantly when the braking resistors are inserted and the energy delivered from the rectifier is absorbed. If the fault is severe, e.g., the three-phase-to-ground fault, the inverter may also output DC current to the braking resistors to release its surplus power, which corresponds to the negative part of the DC current of the inverter. The rectifier side is only minimally affected, as the braking resistors compensate well for the decrease of the power consumption of the inverter during the fault. The fluctuations in the DC current and active power of the rectifier, as well as the sending-end AC voltage, are relatively small. After the fault is cleared, the system can return to steady-state operation rapidly. Overall, the proposed system can cope with different temporary

faults of the receiving-end AC grid.

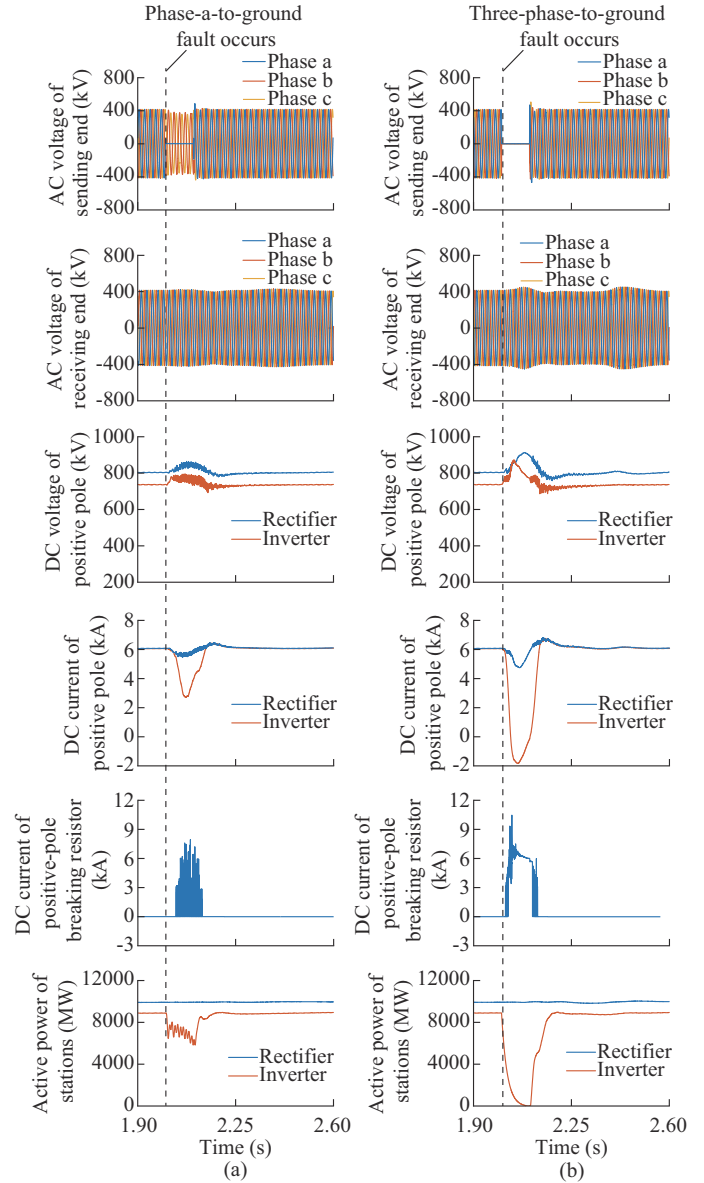


Fig. 14. System responses to receiving-end AC faults. (a) Scenario 1: phase-a-to-ground fault. (b) Scenario 2: three-phase-to-ground fault.

E. DC Fault

The DC faults are assumed to occur at the DC side of the rectifier, the midpoint of the DC lines and the DC side of the inverter, and the system responses are shown in Fig. 15. In all scenarios, the solid pole-to-ground faults occur at $t=2$ s at the positive pole, before which the system operate stably. The fault duration is 100 ms. The upper and lower thresholds for the AC braking resistors used to maintain the submodule capacitor voltage of the parallel MMC are 1.1 p.u. and 1.05 p.u., respectively.

According to Fig. 15, the DC fault current can be controlled to be zero by the hybrid-submodule MMCs in different scenarios, requiring a response time of approximately 200 ms at most. Once the fault has been cleared and the insulation at the fault point has been restored, the system can

return to steady-state operation quickly. The non-fault pole is able to maintain power transmission during the fault. Since the AC dynamic braking resistors at the sending-end AC grid can dissipate the surplus power of the fault pole, the system does not experience serious overvoltage or overcur-

rent during this process. In addition, with the power balance control, there is no unbalanced power between the positive and negative poles following a fault recovery. Overall, the proposed system can cope with temporary DC faults successfully.

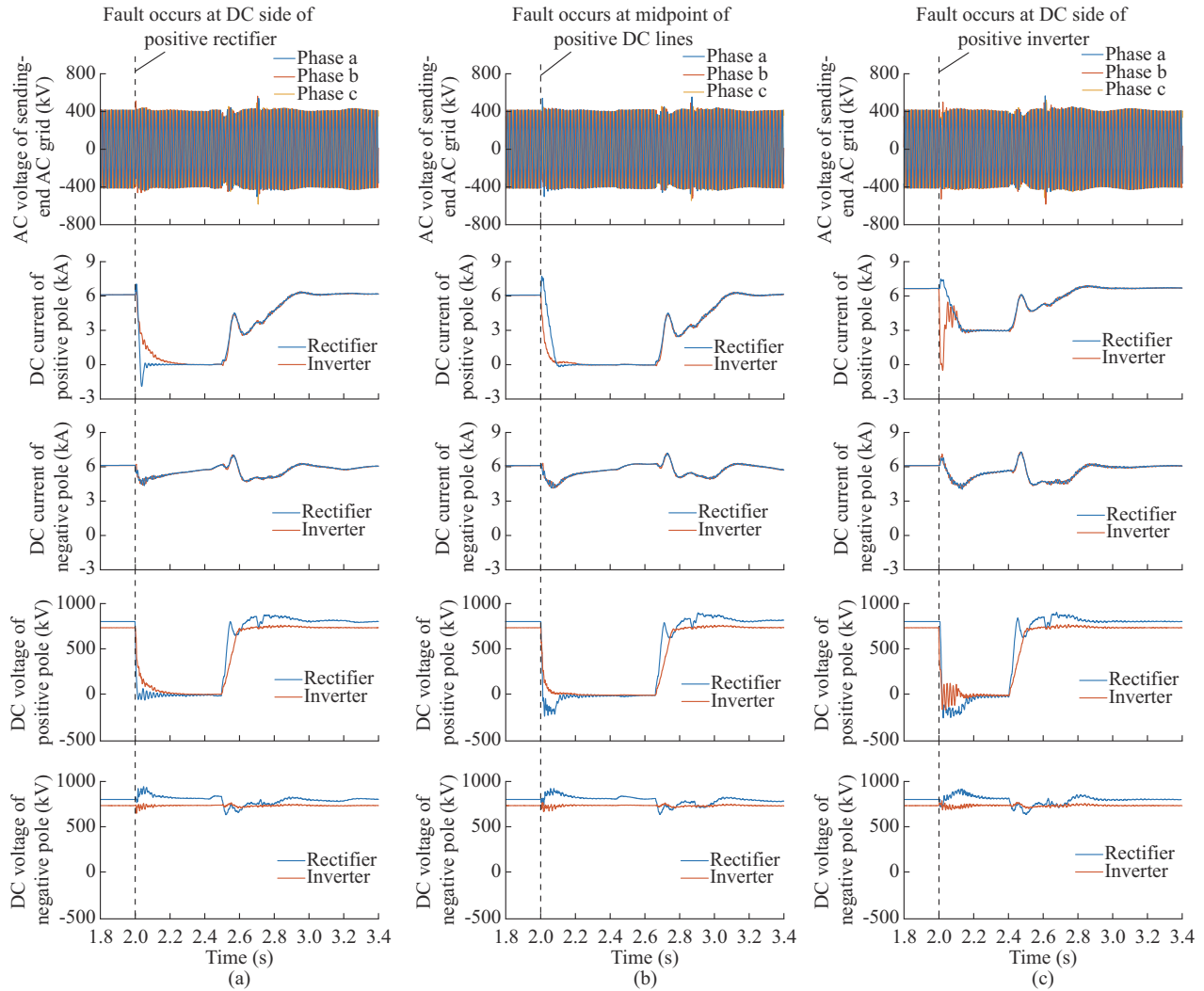


Fig. 15. System responses to positive-pole DC faults. (a) Scenario 1: fault at DC side of positive rectifier. (b) Scenario 2: fault at midpoint of positive DC lines. (c) Scenario 3: fault at DC side of positive inverter.

V. CONCLUSION

This paper proposes a novel parallel converter-based hybrid HVDC system for the integration and delivery of large-scale renewable energy. The main conclusions are summarized as follows.

1) By paralleling the low-capacity MMC at the rectifier side, the system can provide voltage support for the sending-end AC grid. This feature makes the proposed system suitable for the integration and delivery of pure REBs.

2) The active power control of the LCC enables it to undertake all the active power transmission on the rectifier side and to absorb the fluctuating active power, thereby fully utilizing its bulk-power transmission capability.

3) The parallel MMC can maintain the reactive power balance of the sending-end AC grid. Besides, it can compensate

for harmonic currents of the LCC with the harmonic current control, significantly reducing the harmonic currents injected into the REB from the rectifier station.

4) The effectiveness of the proposed fault ride-through strategies is verified by the simulations. No severe overvoltage or overcurrent occurs during these processes. Besides, the MMCs at both terminals can remain unlocked under various faults, which mitigates the impacts of the faults and ensures continuous voltage support for the REB.

The proposed system also has some limitations. Firstly, although the capacity of the sending-end MMC is significantly reduced, the number of its submodules is still high to withstand the DC voltage. In addition, this paper only discusses the basic operating principles and designs the steady-state and fault ride-through strategies. The stability characteristics

of the system under small and large disturbances still need to be further investigated. These issues will be studied in our future work.

REFERENCES

- [1] W. Wang, G. Li, and J. Guo, "Large-scale renewable energy transmission by HVDC: challenges and proposals," *Engineering*, vol. 19, pp. 252-267, Dec. 2022.
- [2] J. M. Maza-Ortega, E. Acha, S. García *et al.*, "Overview of power electronics technology and applications in power generation transmission and distribution," *Journal of Modern Power Systems and Clean Energy*, vol. 5, no. 4, pp. 499-514, Jul. 2017.
- [3] X. Cai, W. Huang, G. Li *et al.*, "Research on operation control strategy of large-scale photovoltaic cluster transmission via grid-forming VSC-HVDC," *Proceedings of the CSEE*, vol. 43, no. 22, pp. 8734-8745, Nov. 2023.
- [4] S. Chuangpishit, A. Tabesh, Z. Moradi-Sharbabk *et al.*, "Topology design for collector systems of offshore wind farms with pure DC power systems," *IEEE Transactions on Industrial Electronics*, vol. 61, no. 1, pp. 320-328, Jan. 2014.
- [5] R. Zhu, X. Zhou, S. Luo *et al.*, "DC current order optimization based strategy for recovery performance improvement of LCC-HVDC transmission systems," *Journal of Modern Power Systems and Clean Energy*, vol. 11, no. 3, pp. 1020-1026, May 2023.
- [6] X. Li, Z. Xu, and Z. Zhang, "Application of MMC with embedded energy storage for overvoltage suppression and fault ride-through improvement in series LCC-MMC hybrid HVDC system," *Journal of Modern Power Systems and Clean Energy*, vol. 11, no. 3, pp. 1001-1013, May 2023.
- [7] R. Rosso, X. Wang, M. Liserre *et al.*, "Grid-forming converters: control approaches, grid-synchronization, and future trends – a review," *IEEE Open Journal of Industry Applications*, vol. 2, pp. 93-109, Apr. 2021.
- [8] Y. Jin, Z. Zhang, Y. Huang *et al.*, "Harmonic filtering and fault ride-through of diode rectifier unit and modular multilevel converter based offshore wind power integration," *IET Renewable Power Generation*, vol. 17, no. 14, pp. 3554-3567, Oct. 2023.
- [9] Z. Xu, Y. Jin, Z. Zhang *et al.*, "Eight typical schemes of offshore wind power transmission and their key technical problems," *Energies*, vol. 16, no. 2, p. 658, Jan. 2023.
- [10] H. Yang, Z. Cai, X. Li *et al.*, "Assessment of commutation failure in HVDC systems considering spatial-temporal discreteness of AC system faults," *Journal of Modern Power Systems and Clean Energy*, vol. 6, no. 5, pp. 1055-1065, Sept. 2018.
- [11] M. A. Perez, S. Ceballos, G. Konstantinou *et al.*, "Modular multilevel converters: recent achievements and challenges," *IEEE Open Journal of the Industrial Electronics Society*, vol. 2, pp. 224-239, Feb. 2021.
- [12] H. Xiao, K. Sun, J. Pan *et al.*, "Review of hybrid HVDC systems combining line communicated converter and voltage source converter," *International Journal of Electrical Power & Energy Systems*, vol. 129, p. 106713, Jul. 2021.
- [13] P. Bakas, L. Harnefors, S. Norrga *et al.*, "A review of hybrid topologies combining line-commutated and cascaded full-bridge converters," *IEEE Transactions on Power Electronics*, vol. 32, no. 10, pp. 7435-7448, Oct. 2017.
- [14] K. Sun, H. Xiao, J. Pan *et al.*, "A station-hybrid HVDC system structure and control strategies for cross-seam power transmission," *IEEE Transactions on Power Systems*, vol. 36, no. 1, pp. 379-388, Jan. 2021.
- [15] W. Xiang, R. Yang, C. Lin *et al.*, "A cascaded converter interfacing long-distance HVDC and back-to-back HVDC systems," *IEEE Journal of Emerging and Selected Topics in Power Electronics*, vol. 8, no. 4, pp. 4109-4121, Dec. 2020.
- [16] Y. Huang, W. Huang, M. Li *et al.*, "Steady-state control strategy of multi-terminal hybrid UHVDC," in *Proceeding of 2017 19th European Conference on Power Electronics and Applications*, Warsaw, Poland, Sept. 2017, pp. 1-10.
- [17] G. Andersson and M. Hyttinen, "Skagerrak the next generation," in *Proceedings of CIGRE*, Paris, France, Jul. 2015, pp. 1-9.
- [18] Z. Xu, S. Wang, and H. Xiao, "Hybrid high-voltage direct current topology with line commutated converter and modular multilevel converter in series connection suitable for bulk power overhead line transmission," *IET Power Electronics*, vol. 9, no. 12, pp. 2307-2317, Oct. 2016.
- [19] Z. Xu, Z. Zhang, and W. Xu, "Research on application of LCC-MMC series hybrid HVDC topology for large scale clean energy base integration," *Power Capacitor & Reactive Power Compensation*, vol. 43, no. 3, pp. 119-126, Jun. 2022.
- [20] W. Xu, Z. Zhang, and Z. Xu, "A hybrid HVDC topology suitable for large-scale pure clean energy power base transmission," *Electric Power*, vol. 56, no. 4, pp. 17-27, Apr. 2023.
- [21] W. Liu, Z. Zhang, and Z. Xu, "Hybrid HVDC transmission scheme of pure renewable energy base," *Acta Energetica Solaris Sinica*, vol. 44, no. 12, pp. 533-543, Dec. 2023.
- [22] X. Li, Z. Xu, and Z. Zhang, "Enhanced ride-through capability under rectifier-side AC fault for series LCC-MMC hybrid HVDC system," *IEEE Access*, vol. 9, pp. 153050-153057, Nov. 2021.
- [23] N. Zhang, X. Li, Z. Zhang *et al.*, "Overcurrent mechanism and suppression control for MMC arms in hybrid cascaded HVDC system," *CSEE Journal of Power and Energy Systems*, doi: 10.17775/CSEEJPES.2022.00460
- [24] Y. Chen and K. M. Smedley, "A cost-effective single-stage inverter with maximum power point tracking," *IEEE Transactions on Power Electronics*, vol. 19, no. 5, pp. 1289-1294, Sept. 2004.
- [25] H. Gan, H. Xiao, and Y. Huang, "Control strategy and capacity selection of DRU-MMC hybrid converter for large-scale offshore wind power," *Automation of Electric Power Systems*, doi: 10.7500/AEPS20230509003
- [26] M. Szechtman, T. Wess, C. V. Thio *et al.*, "First benchmark model for HVDC control studies," *Electra*, vol. 135, no. 4, pp. 54-73, Apr. 1991.
- [27] *IEEE Standard for Harmonic Control in Electric Power Systems*, IEEE Standard 519-2022, pp. 1-31, Aug. 2022.

Hanlin Guo received the B.S. degree in Shandong University, Jinan, China, in 2020. He is currently pursuing the Ph.D. degree in Zhejiang University, Hangzhou, China. His research interests include high-voltage direct current (HVDC) transmission and grid integration of renewable energy.

Zheren Zhang received the B.S. and Ph.D. degrees in electrical engineering from Zhejiang University, Hangzhou, China, in 2011 and 2016, respectively. He is now with the Department of Electrical Engineering, Zhejiang University. His research interests include HVDC, flexible AC transmission systems, and grid integration of renewable energy.

Zheng Xu received the B.S., M.S., and Ph.D. degrees in electrical engineering from Zhejiang University, Hangzhou, China, in 1983, 1986, and 1993, respectively. He has been with the Department of Electrical Engineering, Zhejiang University, since 1986, and has been a Professor there since 1998. He is a Fellow of IEEE for his contributions to control and modeling of modular multilevel converter (MMC) based HVDC transmission systems. His research interests include HVDC transmission, power system dynamics, and grid integration of renewable energy.